The United Nations University

GEOTHERMAL TRAINING PROGRAMME
Orkustofnun, Grensásvegur 9,
IS-108 Reykjavík, Iceland

Reports 2000
Number 4

ANALYTICAL AND NUMERICAL MODELLING OF COLD WATER INJECTION INTO HORIZONTAL RESERVOIRS

Hennadiy Chetveryk,
Institute of Engineering Thermophysics,
Ukrainian National Academy of Sciences,
03157, 2a Zhelyabov str., Kiev,
UKRAINE
ge_2002@yahoo.com

ABSTRACT

For reasons of environmental protection, reinjection of produced geothermal fluid after use is an important component of most geothermal projects in Ukraine. The geothermal reservoirs will cool down due to the reinjection. Therefore, the temperature of production wells may decrease. This problem can be avoided by a proper location of injection wells in order to minimise the cooling of production wells. For this purpose several analytical and numerical models of 1-, 2- and 3-D reservoirs are presented in this paper. The study shows that there is a good correlation between the analytical and the numerical models, obtained by applying the TOUGH2 simulator. Numerical dispersion was, however, of concern when simulating moving temperature fronts in the reservoir, but was minimised by increasing substantially the number of model elements. Tracer and thermal breakthrough times obtained by numerical modelling confirm the well known fact that chemical breakthrough occurs much earlier than thermal breakthrough. Finally, a safe distance between injection and production wells appears to be in the range 500-1000 m estimated by a 3-D numerical model. All the above modelling conclusions need to be recalculated when more reservoir data becomes available in Ukraine.

1. INTRODUCTION

Ukraine has a long-standing history of geothermal utilization, although not widely known within the international geothermal community. A substantial number of wells has been drilled, yielding geothermal fluids and showing downhole temperatures ranging from 60 to 210°C. Many of the low temperature wells are highly productive, yielding a few tens of litres per second of artesian flow. Interest is now growing for additional development of this sustainable and environmentally benign resource in Ukraine, primarily for space heating purposes.

There are presently three main prospective geothermal areas in Ukraine (Figure 1). These are the Crimean peninsula, the Carpathian region and the Dneper-Donetsk depression. The Crimean peninsula and the Dneper-Donetsk depression consist of sedimentary formations whereas the

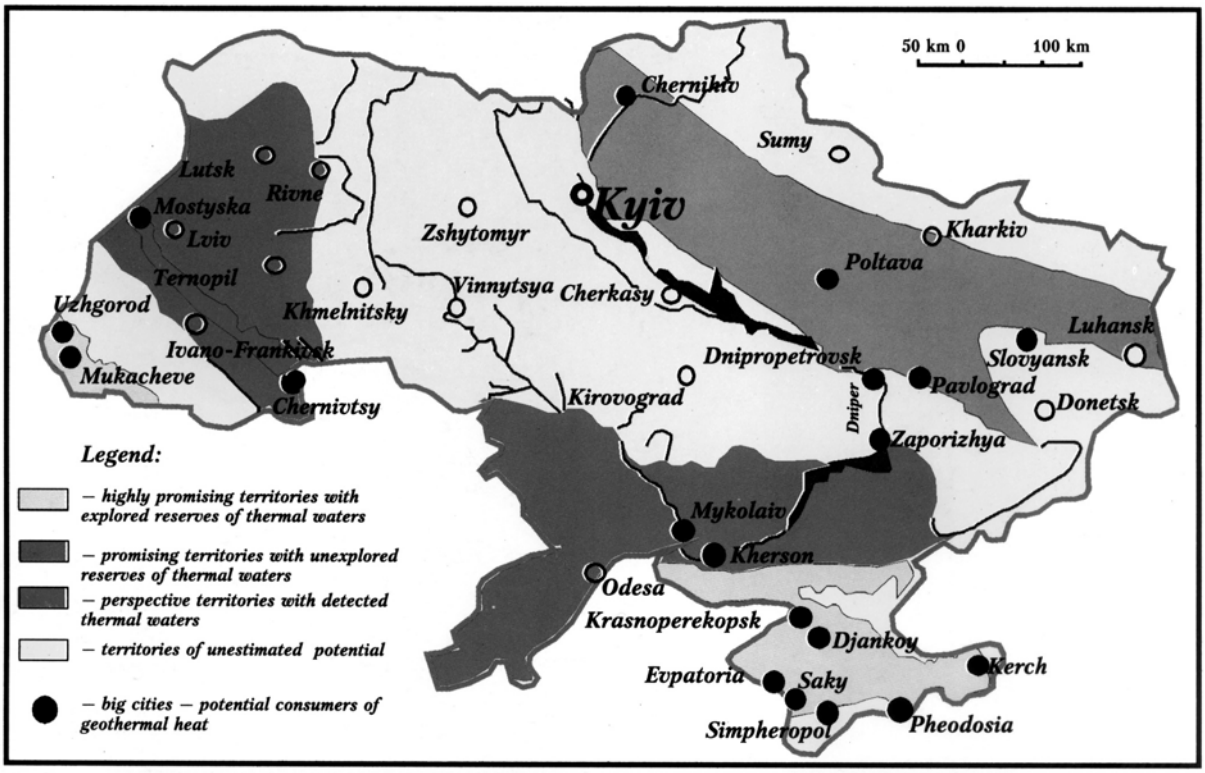

FIGURE 1: Map of Ukraine and its geothermal reserves (Institute of Engineering Thermophysics, 1997)

Carpathian region is fracture-dominated. Geothermal projects in these regions are all carried out by the Institute of Engineering Thermophysics under the programme "Ecologically clean geothermal energy in Ukraine", which started in 1991. Of special interest has been the disposal (reinjection) of wastewater for environmental reasons. Furthermore, reinjection should also be attractive as a means of increasing or sustaining the production potential of the geothermal systems to be utilised. This is not a straightforward task since reinjection may lead to cooling of production wells. Therefore, the location of injection and production wells must be done properly in order to avoid thermal interference.

In the following report several analytical and numerical models of heat and mass in the subsurface are studied in order to better understand the thermal character of production/injection well dipoles. The models all use the same conceptual reservoir model, i.e. a confined horizontal system where hot water is produced from one well and cold water injected into another. The structure of the report is as follows. In Chapter 2 different analytical 1- and 2-dimensional models of heat and mass flow are considered. In Chapter 3 the output of numerical modelling is compared with analytical modelling. The numerical models are, furthermore, used to track the flow of tracers and to predict the influence of seasonal cycling in production for the geothermal reservoir. In Chapter 4 numerical 3-D models for 2 configurations of injection and production wells are considered and the location of thermal fronts in such systems predicted. Figure 2 shows a sketch of the reservoir models studied. A frequent reference will be made to this figure in later chapters.

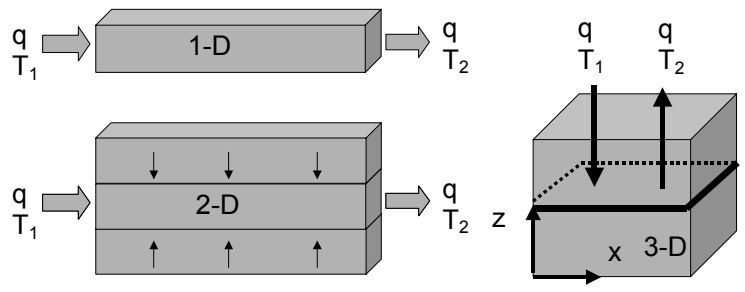

FIGURE 2: A sketch of the 1-, 2- and 3-D reservoir models studied in this report

2. ANALYTICAL MODELS OF HEAT AND MASS FLOW

In this chapter, three reservoir model cases are presented. For all of them an analytical solution for temperature distribution in time and space has been defined. These solutions were derived earlier by the author in Ukraine (Zabarny et al., 1998).

2.1 Case A: 1-D model neglecting conductive heat flow

Suppose that fluid is injected at a rate q (kg/s) from time t=0 into a horizontal reservoir of thickness h (m) and constant cross-sectional area A (m^2). Assume, furthermore, that the influence of the rock matrix and heat conduction can be neglected. In this case the reservoir has a very simple geometry and governing equation for heat flow. The temperature of the injected fluid is T_2 and the initial temperature of the reservoir is T_1. Porosity of geothermal reservoir is ϕ. We also assume isotropic and homogeneous properties of the reservoir. Impermeable layers of zero thermal conductivity surround the reservoir. The model, therefore, considers only 1-D convective flow of mass and heat. A sketch of the geothermal reservoir is shown in Figure 2 (top, left). In order to define its temperature as a function of time and distance from the injection well, we must solve the differential equation presented in Equation 1 with the given boundary and initial condition (Zabarny et al., 1998):

$$<c\rho>\frac{\partial T}{\partial t} + c_w \rho_w V \frac{\partial T}{\partial x} = 0 \qquad with \quad T(x,0) = T_1 \quad and \quad T(0,t) = T_2 \tag{1}$$

where $<c\rho>$ = $\phi\, c_w\, \rho_w + (1-\phi)\, c_r\, \rho_r$ = Average volumetric heat capacity of the reservoir;
V = $q / (\rho_w A\, \phi)$ = True velocity of the injected fluid.

Solving Equation 1 results in the step function:

$$T(x,t) = \begin{cases} T_1 & if \quad x > \dfrac{c_w \rho_w}{<c\rho>} Vt \\ T_2 & if \quad x < \dfrac{c_w \rho_w}{<c\rho>} Vt \end{cases} \tag{2}$$

where x = $(c_w\rho_w/<c\rho>)\, Vt$ defines the location of the cold water temperature front at any time t.

A typical set of reservoir parameters based on Ukrainian data are presented in Table 1. These data are inserted in Equation 2 to give the result for a hypothetical geothermal reservoir presented in Figure 3.

TABLE 1: Parameters used for model case A

Parameter	Value	Unit
c_w	4200	J/(kg °C)
ρ_w	995.7	kg/m^3
c_r	1000	J/(kg °C)
ρ_r	1900	kg/m^3
Q	20	kg/s
ϕ	10	%
A	10000	m^2
T	1000	Day
T_1	80	°C
T_2	30	°C

2.2 Case B: 1-D model with conductive heat flow

The next model considers both convective and conductive 1-D flow in the same simple geothermal reservoir but again only in the horizontal X direction (Figure 2, top, left). In order to define temperature at all distances x and times t, Differential Equation 3 has to be solved with the given boundary and the initial conditions (Zabarny et al., 1998):

$$<c\rho>\frac{\partial T}{\partial t} + c_w \rho_w V \frac{\partial T}{\partial x} = <\lambda>\frac{\partial^2 T}{\partial x^2} \qquad with \quad T(x,0) = T_1 \quad and \quad T(0,t) = T_2 \tag{3}$$

where $<\lambda> = \lambda_w \phi + \lambda_r (1-\phi)$ is the average thermal conductivity in the reservoir (see nomenclature).

Solving the problem defined by Equation 3 gives

$$\theta(x) = 1 - \frac{1}{2}\left(erfc\left(\frac{x - \frac{c_w \rho_w}{<c\rho>} Vt}{2\sqrt{\frac{\lambda_m}{c_r \rho_r} t}}\right) + erfc\left(\frac{x + \frac{c_w \rho_w}{<c\rho>} Vt}{2\sqrt{\frac{\lambda_m}{c_r \rho_r} t}}\right) e^{\frac{c_w \rho_w V x}{\lambda}} \right) \tag{4}$$

where $\theta(x) = (T(x,t) - T_2)/(T_1 - T_2)$ is dimensionless temperature;
erfc (x) $= 1 - erf(x)$ is the complimentary error function; and

$$erf(x) = 2/\sqrt{\pi} \int_0^x e^{-x^2} dx.$$

Table 2 presents the hypothetical parameters used to demonstrate this simple, 1-D horizontal model case, and Figure 3 shows the calculated temperature distribution as a function of distance from the injection point, after 1000 days of continuous injection.

TABLE 2: Parameters used for model case B

Parameter	Value	Unit
c_w	4200	J/(kg °C)
ρ_w	995.7	kg/m^3
c_r	1000	J/(kg °C)
ρ_r	1900	kg/m^3
Q	20	kg/s
ϕ	10	%
A	10000	m^2
T	1000	day
λ_r	3	J/(s m °C)
λ_w	0.7	J/(s m °C)
T_1	80	°C
T_2	30	°C

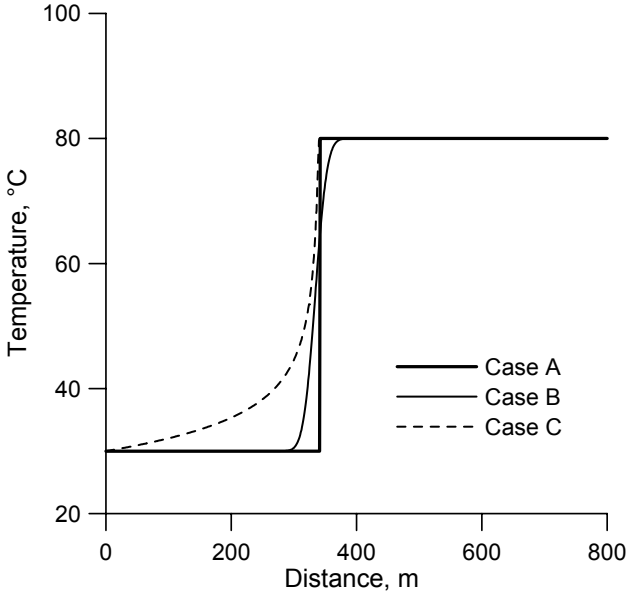

FIGURE 3: Analytical solutions for temperature as a function of distance from injection well for model cases A-C. Cold water injection of 30°C temperature has been continuous for 1000 days

2.3 Case C: 2-D model with vertical and horizontal heat and mass flow

Model cases A and B have the flaw of neglecting vertical heat flow from the confining beds into the reservoir layer studied. As a last analytical model case we, therefore, set up an additional differential equation to account for this important heat transfer mechanism in a geothermal reservoir. A similar problem with the injection of hot water was solved by Lauwerier (1955). The reservoir model selected here is shown in Figure 2 (lower, left).

Assume that $T(x,t)$ defines the temperature within the permeable layer and $T_m(x,z,t)$ is the temperature of the confining beds. Furthermore, $T(\infty,\infty,t) = T_2$ and $T(x,y,0) = T_1$. The heat transfer between the reservoir and the confining beds is presented by Equation 5 and within the reservoir by Equation 6:

$$<c\rho>\frac{\partial T}{\partial t} + c_w \rho_w V \frac{\partial T}{\partial x} = \frac{\lambda_m}{h}\frac{\partial T_m}{\partial z} \tag{5}$$

$$<c\rho>\frac{\partial T}{\partial t} + c_w \rho_w V \frac{\partial T}{\partial x} = <\lambda>\frac{\partial^2 T}{\partial x^2} \tag{6}$$

Initial and boundary conditions are finally given by Equations 7-9 (Zabarny et al., 1998):

$$T(x,0) = T_1 \quad and \quad T(0,t) = T_2 \tag{7}$$

$$T_m(x,z,0) = T_1 \tag{8}$$

$$T_m(x,z,t) = T_1; \quad x \to \infty, \quad z \to \infty \tag{9}$$

Solving the problem defined by Equations 5-9 gives

$$\theta(x,t) = \begin{cases} erf\left(\dfrac{\dfrac{\lambda_m}{c_w \rho_w}\dfrac{x}{V}}{h\sqrt{\dfrac{\lambda_m}{c_m \rho_m}\left(t - \dfrac{<c\rho>x}{c_w \rho_w V}\right)}} \right) & if \quad t > \dfrac{<c\rho>x}{c_w \rho_w V} \\ 1 & if \quad t < \dfrac{<c\rho>x}{c_w \rho_w V} \end{cases} \tag{10}$$

Hypothetical input data for the analytical 2-D model with conductive and convective flow are presented in Table 3, and the computed results are shown in Figure 3 together with the analytical model cases A and B. Comparison between the analytical model cases shows that conductive heat flow is minor compared to the convective heat flow. All models predict similar thermal breakthrough time. But also noticeable is the tail of gradual upwarming by vertical heat flow for the 2-D model case C. This means that cooling rates after thermal breakthrough are much slower here than for cases A and B.

TABLE 3: Parameters used for model case C

Parameters	Values	Units
c_w	4200	J/(kg·°C)
ρ_w	995.7	kg/m^3
c_r	1000	J/(kg·°C)
ρ_r	1900	kg/m^3
Q	20	kg/s
ϕ	10	%
A	10000	m^2
T	1000	Day
λ_m	3	J/(s·m·°C)
H	100	M
T_1	80	°C
T_2	30	°C

3. NUMERICAL MODELLING

Cases A-C presented in Chapter 2 are rare examples of non-isothermal reservoir models, which can be solved by analytical methods. Furthermore, the reservoir geometry is highly simplified and hardly to be encountered in nature. Due to the non-linear nature of the governing equation describing heat and mass flow in the subsurface, some type of numerical modelling is most often applied for more complicated reservoir studies.

In the following chapter the simple model cases A-C are re-computed, but this time with the numerical simulator TOUGH2. In addition to temperature predictions, examples of chemical (tracer) breakthrough curves are presented as well as the effect of cyclical (seasonal) production.

3.1 The TOUGH2 numerical simulator

The numerical solutions presented here were generated by the TOUGH2 computer program. TOUGH2 is a numerical simulator for non-isothermal flows of multi-component, multiphase fluids in one, two, and three-dimensional porous and fractured media (Pruess et al., 1999). The basic mass- and energy balance equations solved by TOUGH2 can be written in the general form

$$\frac{d}{dT}\int_{V_n} M^k dV_n = \int_{\Gamma_n} F^k \times n d\Gamma_n + \int_{V_n} q^k dV_n \qquad (11)$$

The integration is over an arbitrary subdomain V_n of the flow system under study, which is bounded by the closed surface Γ_n. Quantity M, appearing in the accumulation term (left hand side), represents mass or energy in the volume element, V_n, with $k = 1, \ldots, NK$ labelling the mass components and $k = NK+1$ the heat component. F denotes mass or heat flux and q denotes sinks and sources. Finally, n is a normal vector on surface element $d\Gamma_n$, pointing inward into V_n.

3.2 Comparison between analytical and numerical models

It is of interest to compare the three previous analytical models with identical models simulated by the computer program TOUGH2. An important feature here is to discretize the model volume into a finite

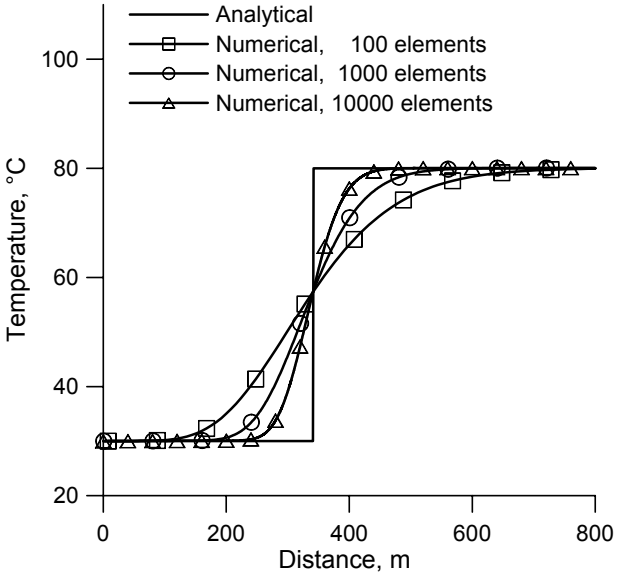

FIGURE 4: Analytical and numerical temperature distribution as a function of distance from the injection well for model case A after 1000 days of injection

number of elements. The 1-D geothermal reservoir was, thus, divided into 100, 1000 or 10,000 elements. A steady state (inactive) element is defined at the downstream end of the numerical grid in order to simulate the acting boundary condition at infinity used for the analytical solutions. Comparison between the analytical and numerical versions of model case A is shown in Figure 4.

An important feature is observed here, namely that the higher the number of model elements, the better match to the analytical solution. This is an expected behaviour and has to do with the volume averaging of temperatures and pressures for each model element performed by TOUGH2 (numerical dispersion). Consequently, the higher the number of grid elements, the better the match to the analytical solution. Note, however, that all the numerical solutions predict correctly the mean location of the thermal breakthrough front.

Numerical dispersion of phase fronts is a well know feature of TOUGH2 (Oldenburg, 1998). Simulating the propagation of phase/thermal/chemical fronts by finite difference methods in strongly advective flow systems is greatly affected by numerical dispersion. Decreasing grid size can diminish numerical dispersion, but this can greatly increase computation times. Another approach for reducing numerical dispersion is to use higher-order differencing schemes but they are unfortunately not supported in the standard release of TOUGH2.

Figure 5 shows the match between the numerical and analytical versions of model case B. Again the numerical diffusion dominates the computed profile, making the effect of conductive heat flow negligible.

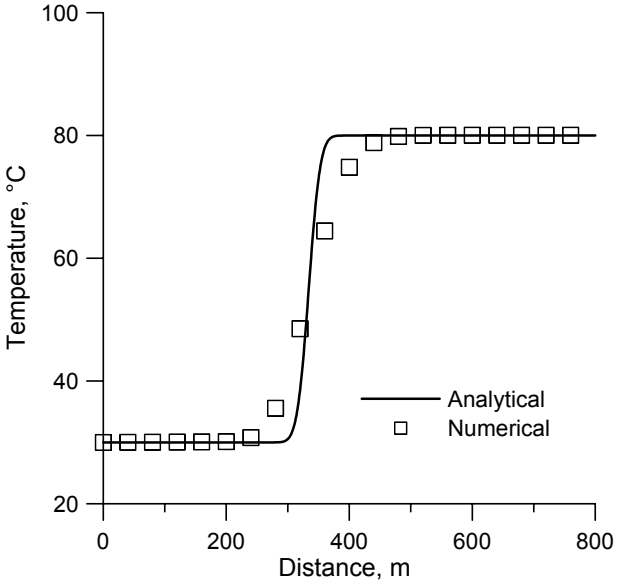

FIGURE 5: Analytical and numerical temperature distribution as a function of distance from the injection well for model case B after 1000 days of injection

TABLE 4: Grid layer thickness in the *Z*-direction for the numerical version of model case C; layer 5 is the reservoir

Number of layer	Thickness of block (m)
1	8
2	4
3	2
4	1
5	10
6	1
7	2
8	4
9	8

For the 2-D model case number C, a special grid was designed in order to simulate the vertical heat flow component. The reservoir was divided into 1000 elements in the X direction and in the Z direction the reservoir was divided as shown in Table 4. Figure 6 finally presents the comparison between the analytical and numerical solutions. The graph shows that a good match is obtained here between the two.

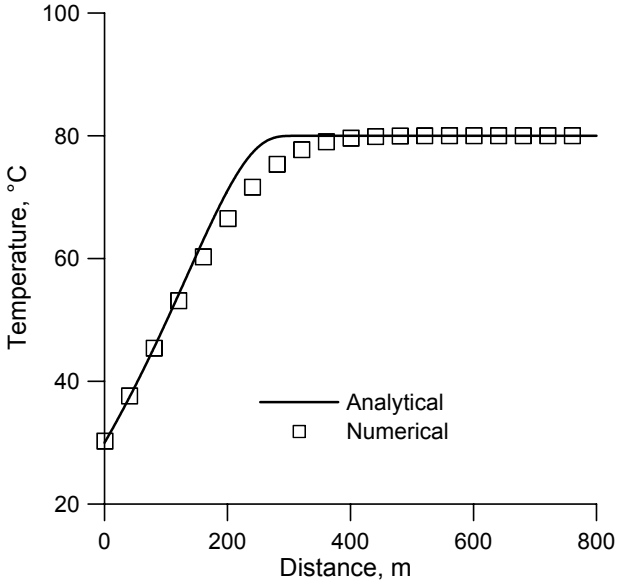

FIGURE 6: Analytical and numerical temperature distribution as a function of distance from the injection well for model case C after 1000 days of injection

3.3 Tracer velocities and concentrations

Tracer tests yield the volume of flow paths in a reservoir and are a powerful method for studying connections between injection and production wells. In general, there is a relationship between chemical and thermal breakthrough times in that thermal breakthrough times are substantially greater than tracer breakthrough times. Tracer tests are often carried out before any significant long-term production is begun in order to predict possible future cooling of the reservoir in response to injection. If diffusion and dispersion processes are neglected, the distribution of injected tracer depends on reservoir permeability and geometry only. It also means that the velocity of a moving tracer in a geothermal reservoir is independent of the thermal properties of rock and fluid.

Tracer tests are generally of two types:

1. Continuous injection of tracer for a long time at a constant flow rate;
2. Continuous injection of water at a constant rate for a long time interrupted by a short period of tracer-water mixture (slug) injection. The idea is to observe how the tracer pulse travels as a function of time and distance away from the injection well.

Figure 7 presents an example of the mass fraction of injected fluid in the 1-D reservoir model cases A and B studied earlier. The figure shows a snap-shot of the concentration of the injected fluid expressed as a percentage of the total pore fluid mass after 200 days of injection. The prediction is based on the two-water feature of TOUGH2 (Pruess et al., 1999). This type of graph is then easily transformed into the corresponding graph of tracer concentration with distance. Assuming that the tracer concentration at the injection point is given by C_0, the tracer concentration at any distance, x, is the product of the mass fraction of the injected fluid times C_0 at that distance.

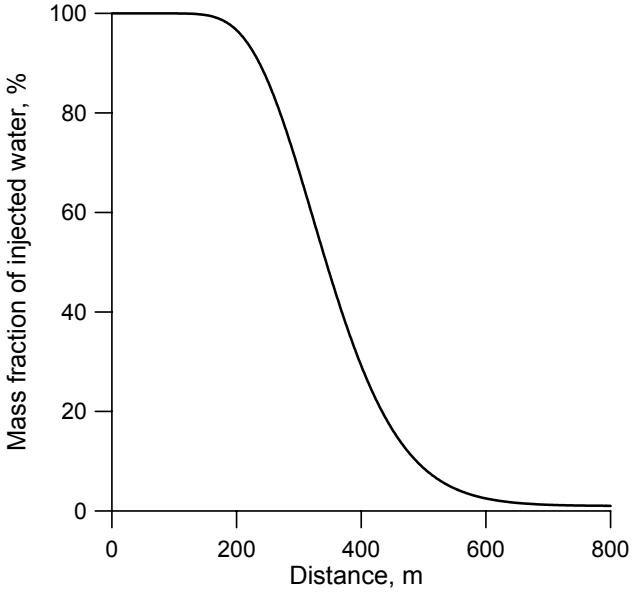

FIGURE 7: Mass fraction of injectate with distance from injection well after 200 days of continuous injection for model cases A and B

Figure 8 shows the history of injected water concentration and reservoir temperature in a model element located 800 m from the injection well, this time for the simple 2-D reservoir model

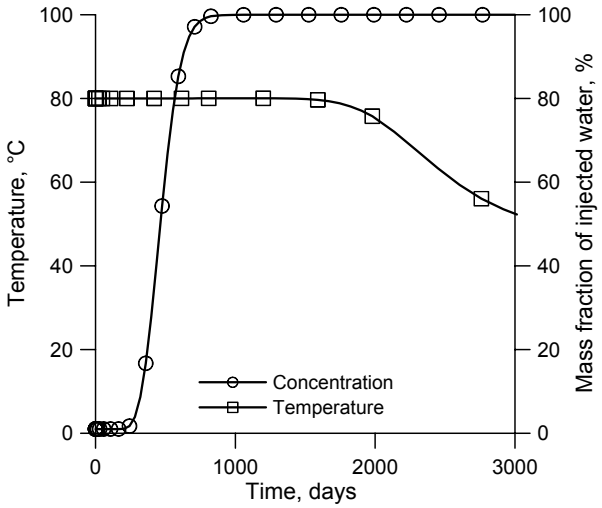

FIGURE 8: Comparison between thermal and chemical breakthrough times for model case C; the point of observation is at 800 m distance from injection point

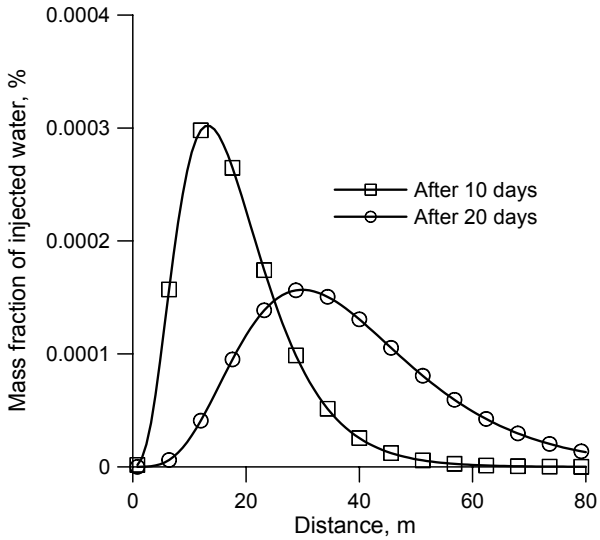

FIGURE 9: Mass fraction of injected water as a function of distance, 10 and 20 days after injection of the tracer slug

case C. The graph clearly illustrates one of the major conclusions drawn from these type of studies, namely that chemical breakthrough times are much shorter than thermal ones. From Figure 8 one can estimate the chemical breakthrough time as 200 days, whereas the thermal breakthrough time is 1750 days.

Figure 9 shows velocity of a moving tracer slug for 1-D model cases A and B. Here we assume that we identify the injectate, mixed with tracer, as water 2. The remaining water in the reservoir is then identified as water 1. The name of the game is then to monitor the concentration of water 2 (X_2) with time and distance and use the results to estimate the concentration of the injected tracer. Figure 9 is based on model cases A and B. At time $t = 0$ water 2 is injected for $t_{inj} = 10$ minutes at 20 kg/s. From then on, only water 1 is injected at the same rate. This slug of water 2 (tracer) then flows out from the injection point, initially as a sharp spike but is then gradually smoothed out due to numerical dispersion. Assuming that X' kg of tracer were injected with water 2, one can define an initial tracer concentration C_o as

$$C_o = \frac{X'}{t_{inj} q} \quad \left[\frac{kg\ of\ tracer}{kg\ of\ water} \right] \tag{12}$$

The tracer concentration at any time or distance is then given by

$$C(x,t) = X_2(x,t)\, C_o \tag{13}$$

The governing equations of thermal and chemical transportation are similar (Stefansson, 1997). It can be shown, however, that whereas the volume of the flow path between the injection and production wells determines tracer breakthrough time, the available surface area determines the thermal breakthrough time. This is due to the effect of heat transfer from the rock matrix to the often random flow channels between the wells. As a result, the speed of the thermal front can be partially determined by the speed of the tracer by making an assumption on the geometry of the flow channels. However, this is not a unique relationship, and there might be cases where the surface area is so large that the thermal front will never reach the production well.

Fear of thermal breakthrough has frequently been the deciding factor against using reinjection in geothermal operations (Stefánsson, 1997). In some case this fear has been justified, but in others it has been based on wrong assumptions and a misinterpretation of field data.

The whole range of possibilities, from injecting outside a well field to injection into the upflow of a reservoir, has been debated. At present, there is no universally accepted rule for the proper location of injection wells. James (1979) has discussed some of the factors involved in reinjection strategy for geothermal reservoirs. He concludes that the first law of reinjection is the following: "Production wells and reinjection wells are interchangeable". According to this law, there are no production wells or injection wells, only wells. This intermixed model assumes that production and injection wells are uniformly distributed in the field.

Tracer tests can provide information about the flow path and the flow velocity of the geothermal fluids between the injection and production wells. This information can be used to predict cooling due to reinjection (Axelsson and Stefánsson, 1999). It is interesting to determine the amount of tracer X' to be injected. Equation 14 describes approximately how to determine this proper amount of tracer:

$$X' = Cq\Delta t_w \tag{14}$$

In Equation 14, C is a desired maximum tracer concentration in observation well, q is the injection rate and Δt_w is width at half height of concentration. The maximum tracer concentration depends on what kind of tracer is to be used and on the background concentration of the same tracer in the geothermal fluid. The tracer should have similar flow and thermal properties as the geothermal fluid, but must differ in properties such as colour, radioactivity or chemical concentration, to allow detection (Liu, 1999). There are three main classes of tracers: dyes, radioactive tracers and chemical tracers.

Sodium-fluorescein is used as a groundwater and geothermal tracer because of its low detection limits, ease of analysis, and strong colour at low concentrations (Adams and Davis, 1991). Bromides and iodide are the most commonly used chemical tracers in geothermal studies, because they are very stable during transport in the reservoir. If iodide is used, C is equal to 1 ppm approximately. If sodium-fluorescein is used, C is equal to 10 ppb approximately. In Equation 14, Δt_w depends on the distance between the injection and production wells and the nature of the connection between the wells. But we do not have any information about the connection between the wells initially. For low-temperature fields, Δt_w ranges approximately from 10 to 30 days for a short distance between injection and production wells (up to 500 m), and from 100 to 300 days approximately for longer distances (1-2 km). Using Equation 14 for a reservoir that has 800 m between the injection and production wells and flow rates of 20 l/s, 1.2 kg of sodium-fluorescein or 12 kg of iodide are needed.

3.4 Cyclical injection rates

It is often necessary to estimate the temperature in a geothermal reservoir when production and injection rates change with time. This applies to Ukraine where space heating is only necessary during winters. Solving the problem analytically is very difficult. Therefore, some type of numerical method must be applied. The following is an example of this, using TOUGH2. In the summer season both production and injection rates are assumed to be 10 kg/s, whereas in winter the corresponding flow rates are 20 kg/s. The injection well is placed at $x = 0$ and the production well at x = 800 m. Also, it is assumed that the summer season is 162 days long in the Carpathian region (Sokolov, 1963).

The two-dimensional model grid for case C is re-used here with the slight modification that the grid is extended in both directions from the two wells. The predicted temperature change with time at 100 m distance from the injection well is shown in Figure 10. Surely this distance is far too short in terms of cooling concern; in less than 2 years the temperature is down to that of the reinjected fluid.

In order to define a safe minimum distance between the injection and production wells, model temperatures at different distances from the injection well were computed. The predicted temperature histories are shown in Figure 11. The figure suggests that a distance of more than 1000 m should be used between injection and production wells if the reservoir geometry is as simple as that of case C.

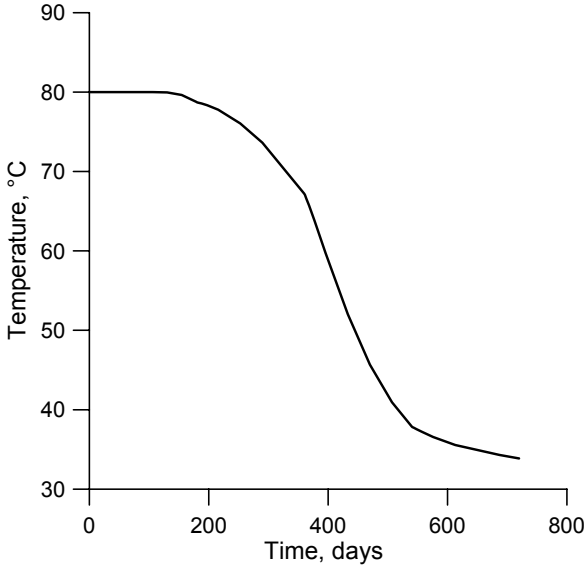

FIGURE 10: Temperature as a function of time at 100 m distance from injection well; model case C and cyclical injection rates

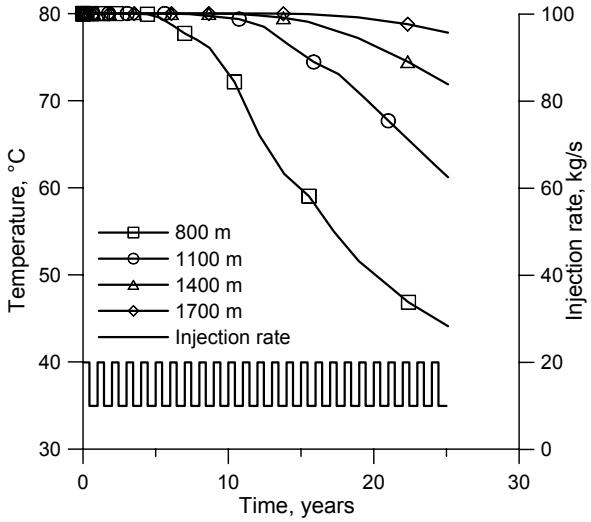

FIGURE 11: Model temperature histories for variable distances between injection and production wells assuming cyclical injection rates and model case C

Figure 12 compares model temperatures for the case of constant 20 kg/s injection compared with the cyclical injection described above and presented in Figure 11. As is to be expected, the cyclical injection results in a much slower cooling of the production well and should, therefore, be preferred in the long term reservoir operation.

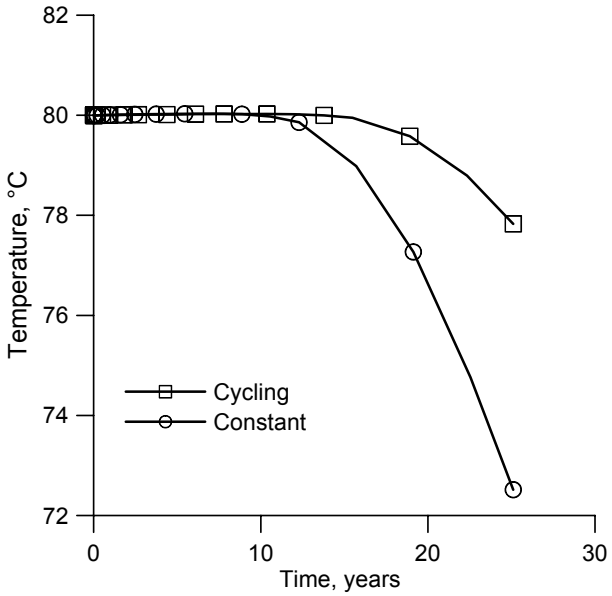

FIGURE 12: Predicted model case C temperature at a distance of 1700 m from injection well for both constant 20 kg/s injection rate and the cyclical injection shown in Figure 11

4. NUMERICAL 3-D MODELS

4.1 Production/injection well dipole

The previous model cases A-C are, in principle, very simple and rarely encountered in nature. As a final example we, therefore, proceed to analyse a 3-D reservoir model similar to the one shown on the right hand side of Figure 2. A horizontal, 100 m thick reservoir layer is assumed, bounded by 3 impermeable, 100 m thick layers from above and below. Figure 13 shows the grid in a horizontal plane. Each layer consists of 18 x 7 elements, thus the total number of elements is 882.

Table 5 presents the rock parameters assigned to the 3-D model. Initially all the model elements are defined at 80°C temperature and 200 bars pressure, except for the inactive (steady state) top and bottom layers. To them initial temperatures of 70 and 90°C are assigned and initial pressures of 170 and 230 bars, respectively. A steady-state condition is then obtained after 1000 years of simulation time.

Figure 14 shows predicted temperatures for several distances between the production and the injection wells. In all cases the production/injection rates are constant, 20 kg/s. Two items are of particular interest in the figure. Firstly that the thermal breakthrough time is on the order of 20 years, even for the 600 m distance. Secondly that a 1000 m separation of the two wells appears comfortable for a long term operation of this well dipole system.

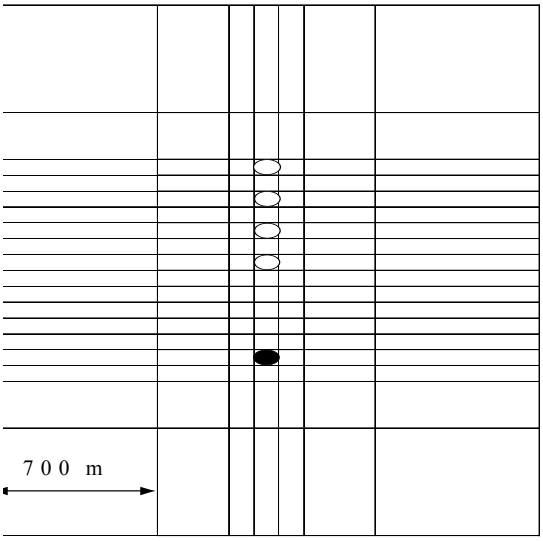

FIGURE 13: Horizontal grid layour for 3-D model; the location of the injection well is shown by a black bullet and the production wells locations are indicated by open circles

TABLE 5: Rock parameters for numerical 3-D model; all elements have thermal conductivity 3 J/sm°C, porosity 10%, heat capacity 1000 J/kg°C and density 1900 kg/m^3

Name of layer	Permeability		
	k_x (m^2)	k_y (m^2)	k_z (m^2)
LAY 1	10^{-15}	10^{-15}	10^{-15}
LAY 2	10^{-50}	10^{-50}	10^{-15}
LAY 3	10^{-50}	10^{-50}	10^{-15}
LAY 4	10^{-12}	10^{-12}	10^{-15}
LAY 5	10^{-50}	10^{-50}	10^{-15}
LAY 6	10^{-50}	10^{-50}	10^{-15}
LAY 7	10^{-50}	10^{-50}	10^{-50}

4.2 Numerical 3-D model with many wells

In geothermal reservoir development, production and injection wells are often sited in more or less regular geometric patterns. The next example demonstrates a 5 spot production/injection model. Their arrangement is shown in Figure 15. The model grid and rock properties are the same as in Table 5.

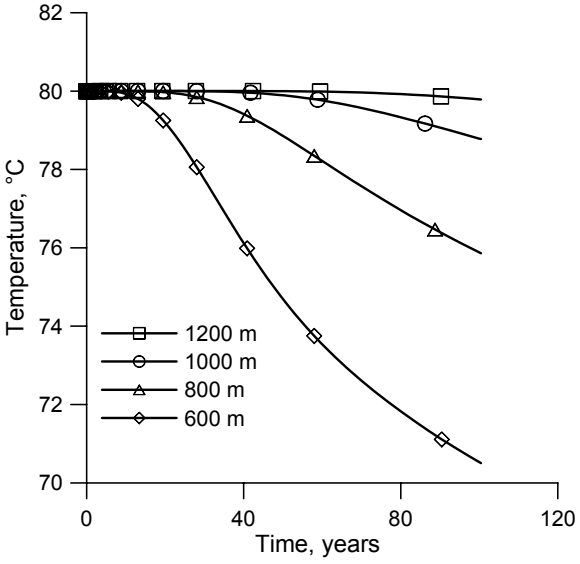

FIGURE 14: Temperature distribution with time for the 3-D model for a few distances between injection and production wells

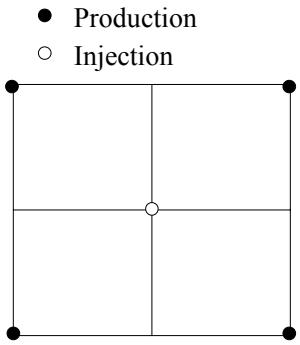

FIGURE 15: A 5 spot injection/production well setup

Figure 16 shows simulated temperature of the centre production well for variable diagonal distance to the 4 injection wells. Very similar cooling pattern in obtained as in Figure 14, but this time all distances are only half of that in Figure 14. This is actually a trivial conclusion and underlines the benefit of distributing the number of injection points as much as possible.

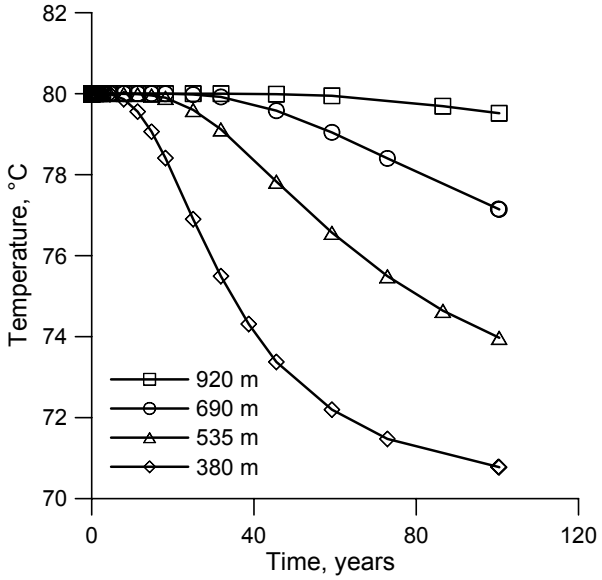

FIGURE 16: Temperature as a function of time for different distances between injection and production wells for a 5 spot well configuration

5. CONCLUSIONS

The main conclusions of this study on cold water injection into horizontal reservoirs are:

1. Reasonable agreement is obtained between analytical and numerical solutions for 3 simplified 1-D and 2-D reservoir cases.
2. Numerical dispersion is, however, a problem when sharp moving fronts are simulated by the integrated finite difference method used in TOUGH2. This problem can be minimised either by increasing the number of grid elements or by applying higher order differencing schemes in the TOUGH2 code itself.
3. Substantially longer thermal than chemical breakthrough times are correctly obtained when applying numerical modelling techniques.
4. The effect of seasonal flowrates in Ukraine has also been predicted by numerical models. This study shows that for a standard injection/production well dipole, substantially slower reservoir cooling is predicted if pumping rates are reduced in summer time compared to what happens if the production is constant throughout the year.
5. Numerical 3-D models for a hypothetical geothermal reservoir suggest that 500-1000 m distance should be kept between injection and production wells in order to maintain reservoir cooling rates at acceptable levels.
6. In the future, when more data becomes available, the above models need to be revisited.

ACKNOWLEDGEMENTS

I would like to thank Dr. Ingvar B. Fridleifsson, director of the UNU Geothermal Training Programme, and Mr. Lúdvík S. Georgsson, the deputy director, for excellent organization and guidance in the training programme and to Mrs. Gudrún Bjarnadóttir for help during my stay in Iceland. Many thanks to my supervisors, Grímur Björnsson and Steinar Thór Gudlaugsson, for their help in preparing the report.

NOMENCLATURE

A = Cross-section of reservoir (m^2);
C = Concentration of tracer at maximum (ppb);
C_o = Initial concentration of tracer in the reservoir (ppb);
c_r = Heat capacity of rock (J/kg°C);
c_w = Heat capacity of water (J/kg°C);
$<cp>$ = Average volumetric heat capacity of reservoir (J/m^3 °C);
h = Thickness (m);
k_x,k_y,k_z = Permeability in X,Y and Z directions, respectively (m^2).
q = Flow rate (kg/s);
T = Temperature in reservoir at x (m) from injected well and t (s) after starting injection (°C);
T_m = Temperature in matrix of rock at x (m) from injection well, z (m) depth and t (s) after injection (°C);

T_1 = Initial reservoir temperature (°C);
T_2 = Temperature of injected water (°C);
t = Time after starting injection (s);
t_{inj} = Time of injected tracer (s);
V = True velocity of the injected fluid (m/s);
X' = Amount of tracer with water 2 (kg);
X_2 = Concentration of water 2;
x,y,z = Coordinate from injected point (m);

λ_w = Thermal conductivity of injected water (J/s m °C);
λ_r = Thermal conductivity of rock (J/s m °C);
λ_m = Thermal conductivity matrix of rock (J/s m °C);
$<\lambda>$ = Average thermal conductivity in reservoir (J/s m °C);
Δt_w = Width at half height of concentration (days);
θ = Dimensionless temperature;
ρ_r = Density of rock (kg/m^3);
ρ_w = Density of water (kg/m^3);
ϕ = Porosity (%);

REFERENCES

Adams, M.C., and Davis, J., 1991: Kinetics of fluorescein decay and its application as a geothermal tracer. *Geothermics, 20,* 53-66.

Axelsson, G., and Stefansson, V., 1999: Reinjection and geothermal reservoir management – associated benefits. *Proceedings of the Workshop on Direct Use of Geothermal Energy, Ljubljana, Slovenia,* 21pp.

Institute of Engineering Thermophysics, 1997: *Geothermal power engineering in Ukraine.* Ukrainian National Academy of Sciences, 4 pp.

James, R., 1979: Reinjection strategy. *Proceedings of the 5th Workshop on Geothermal Reservoir Engineering, Stanford University, Stanford Ca,* 323-329.

Lauwerier, H.A., 1955: The transport of heat in oil layer caused by the injection of hot fluid,. *Appl. Sci. Res., Sect. A, 5-2/3,* 145-150.

Liu Jiurong, 1999: Reinjection and tracer tests in the Laugaland geothermal field, N-Iceland. Report 6 in: *Geothermal Training in Iceland 1999.* UNU, G.T.P., Iceland, 141-164.

Oldenburg, C.M., 1998: Higher-order differencing for phase-front propagation in geothermal systems, *Proceedings of the 23th Workshop on Geothermal Reservoir Engineering, Stanford University, Stanford, CA,* 127-134.

Pruess, K., Oldenburg, C., and Moridis, G., 1999: *TOUGH2 User's Guide Version 2.0,* Lawrence Berkeley National Laboratory, 197 pp.

Sokolov, E.Y., 1963: *Heat supply and thermal network.* Government Power Publish., Moscow, 310 pp.

Stefánsson, V., 1997: Geothermal reinjection experience. *Geothermics. 26,* 99-139.

Zabarny, G.M., Shurchkov, A.V., and Chetveryk, H.O., 1998: *The computer programs for calculation of some parameters of geothermal systems.* Institute of Engineering Thermophysics, Ukrainian National Academy of Sciences, Kiev, 126 pp.